Supplemental Data

Materials and Methods

Participants were recruited and studied between April 2010 and March 2016.

Participants

The injury mechanisms for our TBI group were as follows: 5 motor-vehicle accident (MVA) – pedestrian, 3 MVA – passenger, 6 fall – skateboard, 2 fall – scooter, 2 fall – bike, 1 fall – skiing, 1 assault, 1 uncategorized blunt head trauma. From the CT scan that participants received at the hospital, the prevalence of CT findings was as follows across the 20/21 participants for whom we had clinical CT data: increased intracranial pressure (15%), diffuse axonal injury (5%), subarachnoid hemorrhage (30%), ventricular hemorrhage (15%), epidural hematoma (45%), subdural hematoma (30%), intracerebral hematoma (50%), contusions (40%), skull fracture – any (65%), depressed skull fracture (30%), non-depressed skull fracture (35%).

Inclusion Criteria: 1) non-penetrating msTBI (intake or post-resuscitation GCS score between 3 and 12 or higher GCS with positive image findings); 2) 8-18 years of age at time of injury; 3) right-handed; 4) normal visual acuity or vision corrected with contact lenses/eyeglasses; and 5) English skills sufficient to understand instructions and be familiar with common words (the neuropsychological tests used in this study presume competence in English).

Exclusion Criteria: 1) history of neurological illness, such as prior msTBI, brain tumor or seizure disorder requiring medication; 2) motor deficits that prevent the participant from being examined in an MRI scanner (e.g. spasms); 3) history of psychosis, ADHD, Tourette's Disorder, learning disability, mental retardation, autism or substance abuse. These conditions were identified by parental report and are associated with cognitive impairments that might overlap with those caused by TBI. Participants were excluded if they had metal implants that prevented them from safely undergoing a MRI scan. Inclusion and exclusion criteria for the healthy controls were the same except for inclusion criterion #1.

Scan Comparison

Half-way through the study, scanning moved from the UCLA Brain Mapping Center (BMC) to the Staglin IMHRO Center for Cognitive Neuroscience (Staglin). Both scanners were 3T Siemens Trio scanners, and the

protocol was maintained. To determine that this scanner change did not introduce bias into our data, we scanned 6 healthy adult volunteers at both the BMC and Staglin centers, 1.5 months apart. We then assessed possible bias in both the T1-weighted images and diffusion-weighted images. Extensive details of this process may be found in a previously published paper [1]. For the T1-weighted images, the scan comparison analyses revealed no detectable pattern in the difference between the intensity correction fields above noise, except in the cerebellum, where there were some scanner induced differences in image intensity even after N3 correction (intensity correction). For this reason, the cerebellum was masked out of the analyses presented in this paper. Twenty-four (12 TBI, 12 control) participants had both scans on the same scanner, while 17 (9 TBI, 8 control) had time 1 and time 2 on different scanners. A concern is that this change in scanner could exaggerate longitudinal changes, as scanner differences are compounded with true longitudinal changes. We made every effort to minimize this effect, through our analyses that revealed no detectable differences in intensity correction fields. We also included scanner as a covariate in all analyses, and we included the 6 volunteers in longitudinal analyses to help control for any effects of scanner differences.

Tractography and Fiber Clustering

Raw HARDI images were visually checked for artifacts, resulting in 2 participants being excluded from all analyses due to extensive slice dropout (not included in above participant count). HARDI images were corrected for eddy-current induced distortions using the FSL tool "eddy_correct" (http://fsl.fmrib.ox.ac.uk/fsl/). DMRI scans were skull-stripped using "BET". FA and MD maps were computed using "dtifit". Whole-brain HARDI tractography was performed with Camino (http://cmic.cs.ucl.ac.uk/camino/). The maximum fiber turning angle was set to 35°/voxel to limit biologically implausible results, and tracing stopped when fractional anisotropy (FA) dropped below 0.2, as is standard in the field.

The Eve atlas was registered, linearly and then non-linearly, to each participant's FA map using ANTs (Advanced Normalization Tools [2]) and its ROIs were correspondingly warped to extract 18 tracts of interest for each participant based on a look-up table [3]. ROI registration was visually checked for all participants, and all passed quality control. Each participant's FA map was further registered non-linearly to each of the 5 manually constructed atlases. All registrations were visually inspected for quality, and all passed quality control. The 18

tracts from each atlas were then warped to the participant space based on the deformation field from the registration steps [4]. We refined fiber extractions of each tract based on the distance between the warped corresponding tract of each atlas and the participant's fiber candidates from ROI extraction. Individual results from the 5 atlases were fused. We visually inspected the resulting fiber bundles.

ERP Recording

Electroencephalography was recorded during the post-acute phase (2-5 months post-injury) while participants completed a computerized, pattern-matching task with bilateral field advantage (see [5]). A BIOSEMI system was used to acquire ERPs. Visual ERPs were recorded, synchronized to the onset of the pattern presentation. The low pass filter = 40Hz, high pass filter = 0.16Hz, bandwidth (3dB) = 134Hz and sample rate = 512Hz. Parietal and occipital electrode sites were used as prior studies found these lateral sites produce large visual ERPs that yield clear evoked potential IHTTs [6-8]. In addition, electrodes were placed above, below, and at the outer cantus of each eye to record eye movements. Electrodes placed on the mastoid bones (i.e., behind the ears) of participants were used as linked-ears references. This reference point provides a more valid estimate of IHTT than mid-frontal reference points [9]. ERPs at each recording electrode from each trial were stored for later averaging.

For each electrode, ERPs were averaged for the 2 x 2 combinations of left visual field (LVF) versus right visual field (RVF). Averaged ERPs were displayed on a computer visual display and the N1 component identified blind to participant group. For each of the parietal or occipital recording electrodes – contingent upon which set provided the most clearly identifiable nodes and peaks – the latency and amplitude of these components were stored for statistical analysis. IHTT was calculated by averaging ERP waveforms at the P3 or O1 (left hemisphere) and P4 or O2 (right hemisphere) electrode sites. Next, the peak latency (in milliseconds) of the early N1 evoked potential components was determined. Then, the latencies of the ipsilateral and contralateral conditions were subtracted to determine the overall IHTT for each visual field. Finally, the RVF and LVF IHTTs were averaged to compute the overall IHTT for each participant. As mentioned, the average of left to right visual field and right to left visual field IHTTs for each participant was used in the remaining analyses. Longer IHTTs indicate slower transfer of visual information across the posterior brain regions. Accuracy of pattern matching was not recorded

in this study. Prior studies have demonstrated that true deficits in IHTT are related to slower reaction times rather than to response accuracy, particularly in individuals with agenesis of the corpus callosum [10, 11]. Studies of hemispheric disconnection report that the splenium transfers visual and visuo-motor information between hemispheres [12].

Lesion Tracing

Lesions were traced using 3D Slicer 4.5.0 (http://www.slicer.org [13]) slice by slice manually on patient's individual T1 - weighted images, in native space, considering the information from FLAIR and T2 sequences by a neuroanatomical expert (RMV). FLAIR and T2 sequences were co-registered and re-sliced to T1. Contours of the lesion were drawn on the outer borders of gliosis and cysts (hypo-intense regions of T1 images) in case there were corresponding changes of intensities in the other sequences. **Figure e1** shows the extent of the lesions in the TBI-slow-IHTT and TBI-normal-IHTT groups, respectively. Each colored area represents the extent of lesions for an individual subject. 9 of 11 TBI-slow-IHTT and 7 of 10 TBI-normal-IHTT participants had lesions detectable by FLAIR and T2.

Cognitive Performance

Our cognitive performance score is a summary measure assessing multiple domains known to be affected in TBI [14]. It is a linear, unit weighted combination of the following age-based standardized or scaled measures: 1) Processing Speed Index from the WISC-IV/WAIS-III [15]; 2) Working Memory Index from the WISC-IV/WAIS-III [15]; 3) Trials 1-5 from the CVLT-C/II [16]; and 4) Trails 4 from the D-KEFS [17]. Further details of our cognitive performance index are found in [18].

Statistical Analysis

Group Differences

AutoMATE yields matrices containing FA, MD, RD, or AD at consistent indices across participants and these are the input for our analyses. For investigating group differences, we run linear regression in the form:

Eq. 1: $WM(i,j) \sim A + \beta_{group} Group + \beta_{age} Age + \beta_{sex} Sex + \beta_{scan-ch} Scan - ch + \beta_{interval} Interval + \varepsilon$

Where WM(i,j) is FA, MD, RD, or AD at any given matrix index, *A* is the constant WM integrity term, the βs are the covariate regression coefficients, and ε is an error term. In this regression, we are including covariates for age,

sex, whether the patient switched scanners between time 1 and time 2 (binary variable) and the interval between time 1 and time 2 (in weeks). Group is a binary dummy variable. All statistical tests are corrected for multiple comparisons using FDR [19] across all points tested.

Longitudinal Changes

As discussed in the results section, we chose to examine changes in average tract measures, rather than point-wise measures. For this, we again ran linear regressions as shown in Eq. 1, with the dependent variable in the equation being average FA, MD, RD, or AD of the 18 tracts examined, rather than element-wise WM integrity. These were again corrected for multiple comparisons using FDR across all tracts.

Cognitive Changes

To examine differences in cognitive scores, we ran *t*-tests to compare means between groups and within groups between time 1 and time 2. To examine correlations between cognitive scores and WM integrity, we ran linear regressions as shown in Eq. 1 with the variable of interest being change in cognitive scores, instead of group, and the outcome measure being change in WM integrity. We also examined whether changes in cognitive scores were correlated with changes in tract average measures. These were again corrected for multiple comparisons using FDR across all tracts.

Figure e-1. Lesion extent in the TBI-slow-IHTT and TBI-normal-IHTT groups.

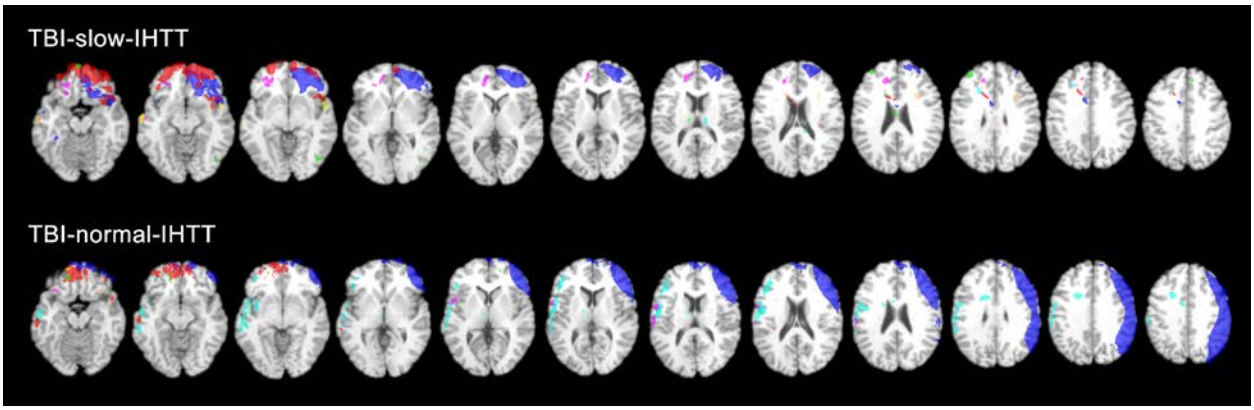

Using FLAIR, T1, and T2 data, lesions were manually traced. Each color delineates lesion extent for a single subject within each group.

Figure e-2. Standard deviation within groups in along-tract mean diffusivity.

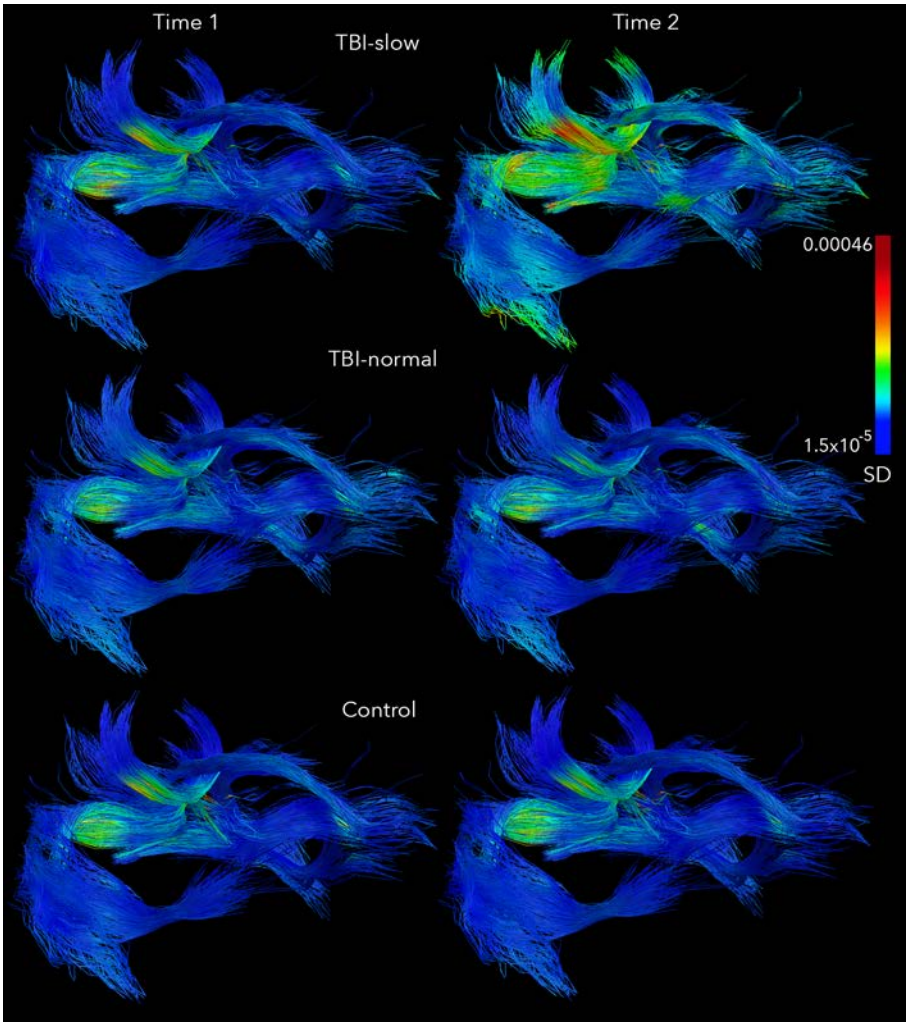

The standard deviation (SD) maps are shown for TBI-slow-IHTT (*N*=11), TBI-normal-IHTT (*N*=10), and healthy controls (*N*=20) for both time points. The SD is display along-tract according to the legend, with blue being areas of low SD and red being areas of high SD.

Table e-1. Group differences in along-tract WM integrity. Element-wise differences in WM integrity between the TBI-slow-IHTT (*N*=11) and control (*N*=20), run using linear regression. For each tract investigated, the percentage of the tract that passed the FDR threshold is given (FDR threshold for TBI-slow-IHTT vs. control FA=0.00118, for MD=0.0190, for RD=0.0129), as well as the minimum *p*-value for group differences on each tract. POCG=postcentral gyrus, PRCG=precentral gyrus, Front.=frontal, Par.=parietal, Occ.=occipital, Temp.=temporal, ATR=anterior thalamic radiation, CGC=cingulum, CST=corticospinal tract, IFO=inferior fronto-occipital fasciculus, ILF=inferior longitudinal fasciculus, ARC=arcuate fasciculus.

	FA		MD		RD		AD	
	% tract sig.	min. *p*	% tract sig.	min. *p*	% tract sig.	min. *p*	% tract sig.	min. *p*
L ATR	2.7	$2.5x10^{-5}$	24.5	$3.6x10^{-7}$	18.5	$9.2x10^{-7}$	-	-
R ATR	9.4	$3.7x10^{-5}$	32.1	$1.3x10^{-5}$	29.3	$4.2x10^{-6}$	-	-
CC Front.	23.2	$1.8x10^{-6}$	33.1	$3.6x10^{-7}$	31	$2.3x10^{-7}$	-	-
CC Occ.	17.1	$2.6x10^{-5}$	44.5	$3.4x10^{-6}$	27.7	$1.4x10^{-5}$	-	-
CC Par.	8.4	0.00011	40.9	$2.3x10^{-6}$	24.1	$3.4x10^{-6}$	1.1	$6.9x10^{-6}$
CC POCG	5.5	0.00015	24.3	$1.8x10^{-5}$	11.3	$1.7x10^{-5}$	-	-
CC PRCG	5.3	$8.0x10^{-5}$	10.8	$8.9x10^{-7}$	6.7	$9.6x10^{-5}$	-	-
CC Temp.	43.5	$1.0x10^{-5}$	45.5	$3.0x10^{-6}$	45.8	$3.8x10^{-6}$	-	-
L CGC	4.6	$4.8x10^{-5}$	30.4	$1.6x10^{-5}$	13.9	$3.0x10^{-5}$	-	-
R CGC	7	$6.2x10^{-6}$	23.7	0.00023	10.9	0.00015	-	-
L CST	3.5	$3.6x10^{-5}$	17.7	$3.2x10^{-6}$	10.6	$2.9x10^{-5}$	-	-
R CST	6.2	$5.4x10^{-5}$	12	$4.1x10^{-5}$	11.7	$4.3x10^{-6}$	-	-
Fornix	11.2	$1.6x10^{-5}$	7.3	0.00081	7.5	0.00054	-	-
L IFO	9.1	$5.6x10^{-6}$	70.1	$6.7x10^{-7}$	42.8	$1.8x10^{-6}$	2.6	$8.6x10^{-8}$
R IFO	8.2	0.00010	60.8	$7.9x10^{-7}$	37.4	$3.3x10^{-6}$	-	-
L ILF	7	$3.1x10^{-5}$	70.6	$2.5x10^{-7}$	36.3	$3.5x10^{-7}$	2	$1.0x10^{-5}$
R ILF	8.4	$1.5x10^{-5}$	58.1	$5.3x10^{-7}$	35.8	$5.1x10^{-6}$	-	-
L ARC	5.7	0.00019	52.2	$1.6x10^{-6}$	32.4	$8.2x10^{-6}$	1.3	$8.3x10^{-7}$

Table e-2. Longitudinal changes in mean diffusivity across TBI-slow-IHTT, TBI-normal-IHTT, and healthy controls. Average MD is shown for all three groups, along with the longitudinal change. We compared the longitudinal changes between groups and found significant differences between TBI-slow-IHTT (N=11) and healthy controls (N=20), *p*-values from the linear regression are shown in the table. We did not find significant differences between TBI-normal-IHTT (N=10) and either of the other two groups, but their averages are included for comparison. Measures are only included for tracts showing significant group differences. POCG=postcentral gyrus, Par.=parietal, Occ.=occipital, Temp.=temporal, ATR=anterior thalamic radiation, CGC=cingulum, IFO=inferior fronto-occipital fasciculus, ILF=inferior longitudinal fasciculus, ARC=arcuate fasciculus.

Tract	TBI-slow			TBI-normal			Control			*p*-value (TBI-slow vs. control)
	T1 avg MD	T2 avg MD	change	T1 avg MD	T2 avg MD	change	T1 avg MD	T2 avg MD	change	
L ATR	1.97E-07	3.47E-06	3.27E-06	3.04E-07	5.73E-07	2.69E-07	-9.88E-08	-1.73E-06	-1.63E-06	0.0128
R ATR	4.34E-08	3.55E-06	3.50E-06	5.37E-07	3.43E-07	-1.94E-07	-3.34E-07	-1.66E-06	-1.32E-06	0.0174
L CGC	1.09E-07	4.67E-06	4.57E-06	-5.09E-07	6.64E-07	1.17E-06	-6.96E-07	-2.29E-06	-1.59E-06	0.0132
L IFO	1.69E-06	4.77E-06	3.08E-06	1.06E-06	1.76E-06	6.99E-07	-1.06E-06	-2.38E-06	-1.33E-06	0.0036
R IFO	2.09E-06	4.27E-06	2.18E-06	7.80E-07	1.18E-06	3.97E-07	-1.09E-06	-2.19E-06	-1.10E-06	0.0196
L ILF	2.14E-06	5.00E-06	2.87E-06	1.53E-06	1.68E-06	1.54E-07	-1.74E-06	-2.53E-06	-7.94E-07	0.0038
R ILF	2.76E-06	4.51E-06	1.75E-06	1.16E-06	1.31E-06	1.56E-07	-1.28E-06	-2.31E-06	-1.03E-06	0.0049
L ARC	1.26E-06	3.23E-06	1.96E-06	7.05E-07	1.49E-06	7.81E-07	-9.35E-07	-1.59E-06	-6.57E-07	0.0066
Fornix	1.14E-05	1.40E-05	2.62E-06	-2.64E-06	-3.25E-06	-6.05E-07	-4.07E-06	-6.94E-06	-2.87E-06	0.0017
CC POCG	8.86E-07	5.00E-06	4.12E-06	-1.08E-06	-1.55E-06	-4.70E-07	-7.16E-07	-2.09E-06	-1.37E-06	0.026
CC Par.	1.17E-06	5.57E-06	4.40E-06	-6.54E-07	-6.96E-07	-4.16E-08	-2.09E-07	-2.65E-06	-2.44E-06	0.0074
CC Temp.	3.09E-06	8.45E-06	5.36E-06	6.11E-08	4.26E-07	3.65E-07	-1.75E-06	-4.01E-06	-2.26E-06	0.011
CC Occ.	2.48E-06	6.40E-06	3.92E-06	7.94E-07	6.12E-07	-1.82E-07	-1.01E-06	-3.33E-06	-2.32E-06	0.021

References

1. Dennis EL, Jin Y, Villalon-Reina J, et al. White matter disruption in moderate/severe pediatric traumatic brain injury: advanced tract-based analyses. NeuroImage: Clinical 2015.
2. Avants BB, Tustison NJ, Song G, Cook PA, Klein A, Gee JC. A reproducible evaluation of ANTs similarity metric performance in brain image registration. NeuroImage 2011;54:2033-2044.
3. Zhang Y, Zhang J, Oishi K, et al. Atlas-guided tract reconstruction for automated and comprehensive examination of the white matter anatomy. NeuroImage 2010;52:1289-1301.
4. Jin Y, Shi Y, Jahanshad N, et al. 3D elastic registration improves HARDI-derived fiber alignment and automated tract clustering. 8th Proc IEEE Int Symp Biomed Imaging. Chicago, IL: IEEE, 2011: 822-826.
5. Ellis MU, Marion SD, McArthur DL, et al. The UCLA study of children with moderate-to-severe traumatic brain injury: Event-related potential measure of interhemispheric transfer time. Journal of neurotrauma 2015;In Press.
6. Andreassi JL, Okamura H, Stern M. Hemispheric asymmetries in the visual cortical evoked potential as a function of stimulus location. Psychophysiology 1975;12:541-546.
7. Brown WS, Jeeves MA. Bilateral visual field processing and evoked potential interhemispheric transmission time. Neuropsychologia 1993;31:1267-1281.
8. Ledlow A, Swanson JM, Kinsbourne M. Differences in reaction times and average evoked potentials as a function of direct and indirect neural pathways. Annals of neurology 1978;3:525-530.
9. Saron CD, Davidson RJ. Visual evoked potential measures of interhemispheric transfer time in humans. Behavioral Neuroscience 1989;103:1115.
10. Lassonde M, Sauerwein H, McCabe N, Laurencelle L, Geoffroy G. Extent and limits of cerebral adjustment to early section or congenital absence of the corpus callosum. Behavioural brain research 1988;30:165-181.
11. Sauerwein H, Lassonde MC. Intra-and interhemispheric processing of visual information in callosal agenesis. Neuropsychologia 1983;21:167-171.
12. Damasio AR, Chui HC, Corbett J, Kassel N. Posterior callosal section in a non-epileptic patient. Journal of Neurology, Neurosurgery & Psychiatry 1980;43:351-356.
13. Fedorov A, Beichel R, Kalpathy-Cramer J, et al. 3D Slicer as an image computing platform for the Quantitative Imaging Network. Magnetic resonance imaging 2012;30:1323-1341.
14. Babikian T, Asarnow R. Neurocognitive outcomes and recovery after pediatric TBI: Meta-analytic review of the literature. Neuropsychology 2009;23:283-296.
15. Wechsler D. Wechsler intelligence scale for children–Fourth Edition (WISC-IV). San Antonio, TX: The Psychological Corporation 2003.
16. Delis DC, Kramer JH, Kaplan E, Ober A. California Verbal Learning Test-Children's Version (CVLT-C) ManualPsychological Corporation. San Antonio 1994.
17. Delis DC, Kaplan E, Kramer JH. Delis-Kaplan executive function system (D-KEFS): Psychological Corporation, 2001.
18. Moran L, Babikian T, Giza C, et al. Predictors of cognitive function following moderate/severe pediatric traumatic brain injury. Submitted 2015.
19. Benjamini Y, Hochberg Y. Controlling the false discovery rate: a practical and powerful approach to multiple testing. Journal of the Royal Statistical Society Series B … 1995.